PHYSICAL REVIEW D

PARTICLES AND FIELDS

THIRD SERIES, VOLUME 28, NUMBER 3 1 AUGUST 1983

Measurement of the branching ratio for the rare decay $\pi^0 \to e^+e^-$

J. S. Frank, C. M. Hoffman, R. E. Mischke, D. C. Moir, J. S. Sarracino, and P. A. Thompson*
Los Alamos National Laboratory, Los Alamos, New Mexico 87545

M. A. Schardt†
Department of Physics, Arizona State University, Tempe, Arizona 85281
and Los Alamos National Laboratory, Los Alamos, New Mexico 87545

(Received 10 August 1982)

This paper reports the details of an experiment designed to detect the decay $\pi^0 \to e^+e^-$ and to measure its branching ratio. The experiment used a beam of 300-MeV/c π^- mesons incident on a liquid-hydrogen target to produce neutral pions in the reaction $\pi^- p \to \pi^0 n$. Electron-positron pairs were detected in a magnetic spectrometer by multiwire proportional chambers. A gas Cherenkov counter provided electron identification. The effective-mass distribution of e^+e^- pairs was decomposed with the aid of a Monte Carlo simulation of the $\pi^0 \to e^+e^-$ signal and background processes. The result is 59 ± 21 events, which corresponds to $\Gamma(\pi^0 \to e^+e^-)/\Gamma(\pi^0 \to \gamma\gamma) = (17 \pm 6 \pm 3) \times 10^{-8}$, where the first error is due to statistics and the second is an estimate of systematic effects. The central value is almost four times the unitarity lower limit while existing calculations generally predict values no larger than twice the unitarity limit.

I. INTRODUCTION

The decay $\pi^0 \to e^+e^-$ has a very small branching ratio. This is not surprising since $\pi^0 \to e^+e^-$ occurs through conventional electromagnetic interactions, but is suppressed by a factor of $\alpha^2(m_e/m_\pi)^2$ relative to $\pi^0 \to \gamma\gamma$, and nonelectromagnetic intermediate states are not expected to be significant. While a precise prediction for the $\pi^0 \to e^+e^-$ branching ratio does not exist, several model-dependent calculations have been reported that tend to constrain the branching ratio to lie between 5×10^{-8} and 10×10^{-8}. Such a rare decay is difficult to observe, but experiments, including this one, have been motivated by the sensitivity of the branching ratio to unexpected contributions to this decay.

Like other pseudoscalar mesons that decay into lepton pairs, $\pi^0 \to e^+e^-$ can proceed through an intermediate state of two virtual photons. [See Fig. 1(a).] The contribution from this process dominates the imaginary part of the amplitude for the decay and leads to an effective minimum branching ratio given to lowest order in (m_e/m_π) by

$$B_{\pi^0} = \frac{\Gamma(\pi^0 \to e^+e^-)}{\Gamma(\pi^0 \to \gamma\gamma)} \geq 2\alpha^2 \left[\frac{m_e}{m_\pi}\right]^2 \left[\ln\frac{m_\pi}{m_e}\right]^2 = 4.75 \times 10^{-8} .$$

This result is called the unitarity lower bound.[1]

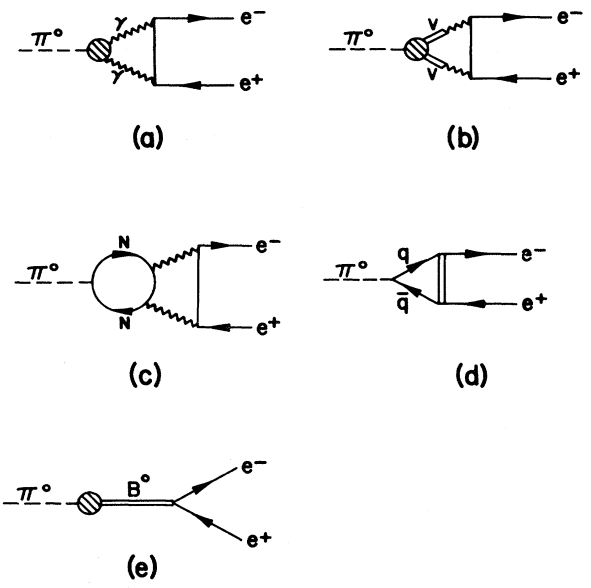

FIG. 1. Diagrams contributing to the decay $\pi^0 \to e^+e^-$: (a) the lowest-order electromagnetic contribution; (b) same as (a) with the contribution due to intermediate vector mesons explicitly shown; (c) same as (a) with the contribution from a nucleon loop shown; (d) leptoquark contribution; and (e) contribution due to a neutral intermediate boson.

 ©1983 The American Physical Society

The calculation of the real part of the amplitude is model dependent. Drell[2] first discussed this decay; his and another early calculation[1] were based on a dispersion relation that involved an unknown cutoff parameter. Later calculations were based on a specific model such as vector dominance[3,4] [Fig. 1(b)], a baryon-loop model[5] [Fig. 1(c)], or, most recently, quark models.[6,7] These models generally predict only small enhancements over the unitarity lower limit. B_{π^0} is also sensitive to nonelectromagnetic lepton-hadron couplings. Direct quark-lepton coupling has been considered[8-11] [Fig. 1(d)] and more recently the exchange of Higgs bosons[12,13] or axions[6] [Fig. 1(e)]. The effect of weak neutral currents appears to be quite small.[11,14]

There was a fifteen-year interval between the first theoretical papers and a publication of an experimental upper limit. Interest in $\pi^0\to e^+e^-$ was prompted by the suggestion of direct quark-lepton coupling[8] since the branching ratio could be enhanced by several orders of magnitude. By looking at existing data on $K^+\to\pi^+e^+e^-$, Davies *et al.*[9] derived an upper limit of

$$B_{\pi^0}<8\times10^{-6}$$

at the 90% C.L. The first experiment[15] designed to look for $\pi^0\to e^+e^-$ studied e^+e^- pairs from $\pi^-p\to\pi^0n$ at rest and obtained

$$B_{\pi^0}<4\times10^{-6}\ (90\%\ \text{C.L.})\ .$$

Another experiment examined e^+e^- pairs from a sample of K^+ decays.[16] They observed about six events consistent with $K^+\to\pi^+\pi^0$, $\pi^0\to e^+e^-$ and reported

$$B_{\pi^0}=(22^{+24}_{-11})\times10^{-8}\ .$$

The central value of this result is almost five times the unitarity limit, but the uncertainty is too large to exclude a value at the unitarity level.

The information from other pseudoscalar decays is not much better. The decay $\eta\to\mu^+\mu^-$ has been observed with a branching ratio

$$B_\eta=\Gamma(\eta\to\mu^+\mu^-)/\Gamma(\eta\to\gamma\gamma)=(5.9\pm2.2)\times10^{-5}$$

in one experiment[17] and

$$B_\eta=(1.7\pm0.6)\times10^{-5}$$

in another.[18] The unitarity limit for this decay gives $B_\eta\geq1.1\times10^{-5}$. The first result is five times the unitarity limit, whereas the second is consistent with this limit. The world-average branching ratio[19] for

$$\Gamma(K_L^0\to\mu^+\mu^-)/\Gamma(K_L^0\to\gamma\gamma)=(1.9\pm0.4)\times10^{-5}\ ,$$

which appears to be larger than the unitarity limit of 1.15×10^{-5}.

Better experiments are clearly needed before any definitive conclusions can be reached about the contribution of the real part of the amplitude for these decays or differences between the amplitudes for the decays of strange and nonstrange pseudoscalar mesons into lepton pairs. The experiment reported here has a large sample of $\pi^0\to e^+e^-$ events. However, the backgrounds in this experiment are substantial and the uncertainty in the determination of B_{π^0} is dominated by the statistical uncertainty in the background subtraction.

In Sec. II, the experimental details are discussed. The data analysis is presented in Sec. III, followed by a description of the Monte Carlo simulation of the experiment in Sec. IV. The results and discussion are contained in Secs. V and VI, respectively.

II. EXPERIMENTAL DETAILS

A. General approach

The decay $\pi^0\to e^+e^-$ can be identified by observing e^+e^- pairs from π^0 decays and showing that their invariant mass equals the π^0 mass. The square of the e^+e^- effective mass is given by

$$M^2=2[m_e^2+(p_+^2+m_e^2)^{1/2}(p_-^2+m_e^2)^{1/2}-p_+p_-\cos\theta_{+-}]\ ,$$

where p_+ and p_- are the lepton momenta and θ_{+-} is the opening angle between the e^+ and e^-. A successful experiment must have sufficient resolution on the measurements of p_+, p_-, and $\cos\theta_{+-}$. The experimental difficulties include the following: (1) the small branching ratio for $\pi^0\to e^+e^-$ requires a large sample of π^0 decays, (2) e^+e^- pairs from backgrounds are unavoidable but must be minimized, and (3) the e^+ and e^- must be identified and momentum analyzed in an apparatus with low mass and high precision.

To obtain a large sample of π^0 decays, we chose to use an intense beam of π^- mesons to produce neutral pions in the reaction $\pi^-p\to\pi^0n$. The actual beam intensity was chosen experimentally to maximize the number of reconstructable events per unit time. The reaction $\pi^-p\to ne^+e^-$ was expected to be an important source of background since the effective mass of e^+e^- pairs from this source form a continuum that extends above m_{π^0}. Guided by a previous study,[20] we concluded that the ratio of the signal to the background from these events with an effective mass near m_{π^0} would be optimized by using an incident π^- momentum of 300 MeV/c and observing π^0 decays in flight.

A dominant source of e^+e^- pairs was the Dalitz decay mode $\pi^0\to e^+e^-\gamma$. Since the Dalitz-decay branching ratio is $\sim10^5$ times that expected for $\pi^0\to e^+e^-$, it was important to suppress these pairs in the design of the trigger. We chose a magnetic spectrometer with multiwire proportional chambers to measure the lepton momenta as well as to suppress backgrounds. The acceptance of our apparatus was optimized for forward-produced π^0's that decayed into an e^+ and e^- with opposite transverse momentum of ~67 MeV/c each. The e^+ and e^- from $\pi^0\to e^+e^-$ usually satisfied this criterion, but most Dalitz decays were eliminated since e^+e^- pairs from Dalitz decay generally have small relative transverse momentum.

Other π^0 decays also contributed background e^+e^- pairs. Decay photons were a source of e^+ or e^- through pair production and Compton scattering. Thus, there were contributions from $\pi^0\to\gamma\gamma$ with both photons converted, $\pi^0\to\gamma e^+e^-$ with one lepton detected and the photon converted, and $\pi^0\to e^+e^-e^+e^-$ where both virtual photons were converted internally. These pairs always had an effective mass less than m_{π^0} because some energy from the π^0 was carried away by undetected e^+ or e^-.

B. Beam and apparatus

1. π^- beam and target

The experiment was performed using the high-energy pion channel (P^3) at the Clinton P. Anderson Meson Physics Facility (LAMPF). The average π^- intensity was 1.8×10^7 π^-/sec at 300 MeV/c with a Δp of ±3 MeV/c; the beam also contained $\sim2\times10^6$ e^-/sec and $\sim2\times10^6$ μ^-/sec. The beam spot was 2.3 cm wide full width at half maximum (FWHM) and 1.5 cm high FWHM at the center of the target. The beam intensity was monitored by an ionization chamber and two scintillation-counter telescopes.[21]

The beam was incident on a liquid-hydrogen (LH_2) target constructed from 0.13-mm-thick Kapton. The target flask was 5 cm in diameter and 25 cm long with hemispherical ends. Twenty layers of 6-μm-thick aluminized Mylar "superinsulation" surrounded the flask. The outer vacuum jacket was an upright cylinder of diameter 33 cm with a "wrap-around" window 12.7 cm high of 0.19-mm-thick Mylar through which the particles exited.

2. Magnetic spectrometer

The magnetic spectrometer is shown in Fig. 2. The magnet had rectangular pole faces 86 cm wide by 44.5 cm deep, separated by a 61-cm gap. The field at the center of the magnet was 0.26 T and the field integral along a typical particle trajectory was 0.238 T m.

Multiwire proportional chambers (MWPC's) were placed on both sides of the magnet to measure trajectories of e^+e^- pairs emanating from the target. In order to detect charged particles close to the beam line, the first MWPC was constructed with a single fiberglass-epoxy outer frame. All other MWPC's had separate frames for the chambers on the left side and the right side of the beam line. The first MWPC had the vertical wires removed in the central region where the π^- beam traversed. The horizontal wires were glued to 1-cm-wide-by-1.5-mm-thick fiberglass-epoxy strips placed on either side of the beam line, positioned 6 cm from the center line and attached to the top and bottom chamber frames. A portion of each wire was then cut away where it crossed the strips to isolate the parts of the wires in the beam region. Signals from the wires to the left and the right of the beam region were read out separately. This technique resulted in a chamber with a deadened central region and with very little material near the beam. The active region of the first chamber was 25.6 cm horizontal by 19.2 cm vertical for each side. The corresponding dimensions of the other chambers were 25.6×25.6 cm, 32.0×51.2 cm, and 64.0×70.4 cm.

Each chamber had horizontal and vertical wires of 20-μm gold-coated tungsten spaced 2 mm apart. The spacing between high-voltage foils was 1.27 cm and they were constructed from 6-μm Mylar with aluminum coating on both sides. The outer windows were 25-μm Mylar for the front chambers and 50 μm for the rear chambers. The gas mixture was 76% argon, 20% isobutane, 0.2% freon, and

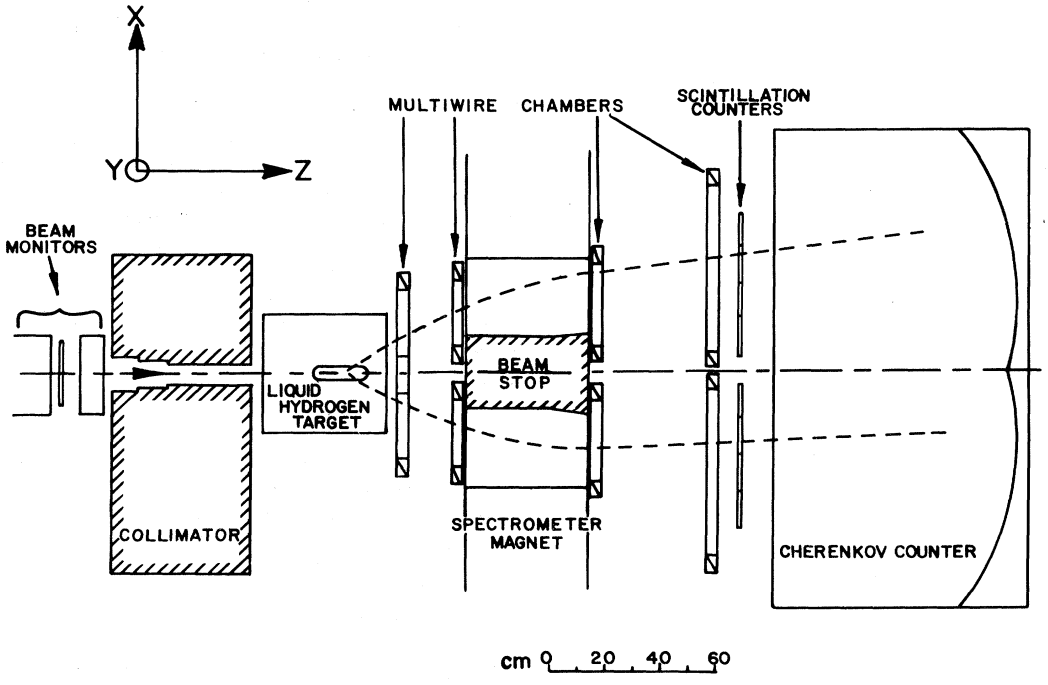

FIG. 2. Plan view of the apparatus to detect $\pi^0\to e^+e^-$ decays. A π^- beam from the left traversed the liquid-hydrogen target and was stopped in a uranium block in the spectrometer magnet. Forward-going particles with a transverse momentum of 67 MeV/c were bent to be parallel to the beam axis by the magnet if they had the correct charges (positive on one side and negative on the other). The scintillation counters provided a trigger and Cherenkov counter identified electrons and positrons.

4% propanol. To handle the high particle fluxes through the chambers in front of the magnet, individual wire readout was used; the lower fluxes in the chambers behind the magnet permitted delay-line readouts for those chambers. Each delay line segment was 12.8 cm wide; in some chambers the edge segment was 6.4 cm wide. Because the tracks passed nearly perpendicular through the chambers, only one or two wires per plane registered per track. If two wires in a front chamber plane registered hits but one or more wires between them did not fire, the hits were considered to be separate. Only one hit could be registered per delay line.

The center of the magnet was filled by a uranium plug, which served as a beam stop for the incident beam. It was 20 cm wide upstream and widened to 30 cm downstream, and was 30 cm deep. 10 cm of lead and 4 cm of carbon preceded the uranium to slow the pions before they interacted in the uranium. An additional 3.2 cm of lead was added on each side of the uranium. This beam stop was adequate to stop the incident pions and prevent most of their secondaries from registering in the rear MWPC's. The volume within the magnet on either side of the plug was filled with helium to reduce multiple scattering and photon conversion. A box filled with helium also was placed between the first and second chambers.

Behind the chambers was a row of eight scintillation counters, each measuring $1.3\times71.1\times13.8$ cm with photomultiplier tubes on top and bottom. Finally, a gas Cherenkov counter provided identification of electrons. A side view of this counter is shown in Fig. 3. The radiator consisted of ~1 m of isobutane at atmospheric pressure. Four aluminum-coated plexiglass mirrors reflected the Cherenkov light to four, 12.5-cm-diameter RCA-8854 phototubes. Each spherical mirror had a radius of curvature of 130 cm and measured 85 cm high and 86 cm wide. On each side of the beam line, one mirror and phototube were located above the median plane and the other set below the median plane.

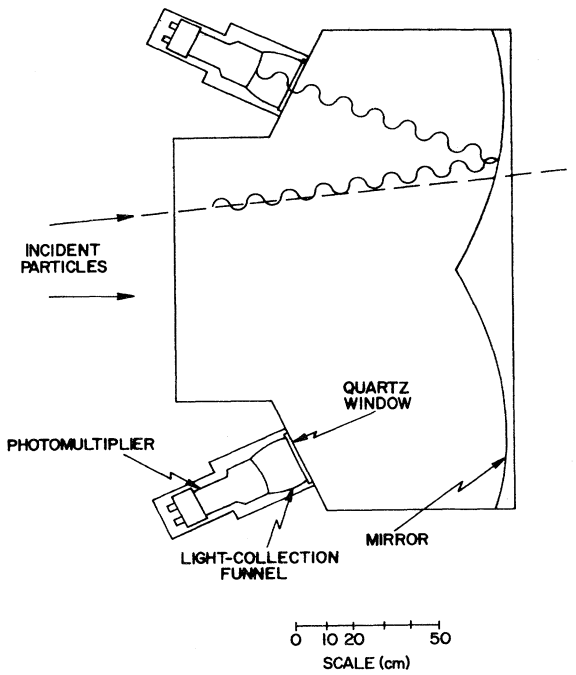

FIG. 3. Cross section of the gas Cherenkov counter showing mirrors and phototubes on one side of the beam.

3. Data collection

The electronics required coincident pulses from a hodoscope counter on each side, from any two of the four Cherenkov counters, and from two of the four front MWPC planes on each side of the magnet. For each trigger the information stored on magnetic tape by an on-line computer consisted of latches for phototubes that fired, pulse-height information from the phototubes, timing information from the phototubes and chamber delay lines, and data from the front wire chambers.

The data set consists of about 100 runs corresponding to a total of $(3.23\pm0.16)\times10^{13}$ incident π^-. This number was determined from the ionization chamber in the beam and has been corrected for beam contamination [$(20\pm2)\%$], π^- decays between the ion chamber and the target [$(6.5\pm0.5)\%$], and the fraction of the beam that missed the target [$(1.5\pm0.5)\%$]. The magnet polarity was reversed regularly to assist in the detection of instrumental asymmetries. In addition to data runs, calibration and test data were taken; these were, for example, runs with the target empty, runs with the magnet turned off, and runs with different trigger requirements.

III. DATA ANALYSIS

The data analysis proceeded in stages. In the first step, all data tapes were processed to eliminate triggers that could not result in analyzable events. This pass eliminated 90% of the triggers simply by requiring (1) hits in three of four chamber planes in each of four coordinates (horizontal and vertical on each side) and (2) a Cherenkov-counter hit on each side of the beam line. This reduction factor was large due to the very loose trigger requirements. The output consisted of 65 416 candidate events.

The first step did not require reconstructing tracks from hits in the chambers. A second step involved determining the locations of the MWPC planes in an absolute coordinate system as described in Sec. III A below. In the next stage of the analysis, the chamber information from the data events was converted into spatial locations and a search for valid tracks was performed. About 40% of the candidate events were found to contain a valid track on each side. In the final analysis stage, various geometrical and kinematical cuts were applied to these events, which resulted in a final data sample of 1330 events.

A. Determination of chamber positions

Several types of information aided in the determination of the MWPC locations. Optical survey measurements were made on all chambers both before and after the experiment. The absolute chamber locations were known to within ±1.5 mm from these measurements. For the delay-line chambers, the true location of a particle was determined from the time difference between the two ends of the delay line. By measuring this time difference and

by knowing the velocity of the signals in the delay line and the zero-time offset of these signals, we were able to calculate the position of the hit within the chamber. The sum of the time measured at the two ends of the delay line was required to lie within a 68-nsec-wide window corresponding to the spread in ion drift time to the MWPC wires.

A collimated ^{55}Fe source mounted on a precision template allowed the first-order time offsets, velocities, and deviations from uniform velocity for each delay line to be determined. However, these chamber constants were found to vary as a function of the amplitude of pulses from the delay lines.

The values for the delay-line constants were refined by fitting straight lines to hits from data taken with the magnet off. Care was taken to reduce the residual field to less than 0.1% of the normal 0.26-T field. For these data, the trigger was modified to require tracks on a single side of the spectrometer. In order to define the centroid of the distributions more precisely, constraints were placed on the quality of the fit in the coordinate orthogonal to the one being examined. This tended to eliminate low-momentum particles that underwent large multiple-scattering deflections. These data also allowed the small relative chamber rotations to be determined.

As another check, we placed a 2-mm-wide Fe target in the beam line and took data with the magnet off in which tracks on both the left and right sides of the spectrometer were required. Requiring the intersection point of these tracks to be at the location of the Fe target provided a constraint on the relative locations of chambers from the two sides and, therefore, on the opening angle. Finally, with the magnet on, we took single-side data that consisted predominately of π's or protons from πp elastic scattering in the LH_2 target. For these data, the known beam momentum provided an additional constraint. An iterative procedure of the reconstruction of these curved trajectories, e^+ and e^- from normal data runs, and the tracks with the magnet off, provided us with the final chamber constants.

We conclude that these final chamber constants determined the relative transverse location of all the chambers on each side of the spectrometer to a precision of ± 0.2 mm. The separation between chamber planes was determined to within an uncertainty of ± 1.5 mm. In addition, since the first chamber contained both sides in a single frame, the separation of the two arms was known to a precision of ± 0.2 mm. The chamber resolutions were determined by comparing distributions of the deviations of hits from the trajectories with those from the Monte Carlo simulation; they will be discussed later.

B. Reconstruction of tracks

An ideal track consisted of four x hits and four y hits. (The coordinate system is defined in Fig. 2.) In general, there were extra hits in some chambers and missing hits in others. This implied that more than one candidate trajectory could be fit to the array of hits. It was the objective of the track reconstruction program to determine the trajectory that gave the best fit to the chamber data. An event was discarded if there were more than eight hits in any single MWPC plane. This cut rejected 4% of the 65 000 candidate events.

In the first step of this process, the x and y coordinates on each side were treated separately. In the vertical projections, tracks were approximately straight lines although some vertical focusing effects were present. All combinations of hits that loosely fit a straight line were accepted. If all four planes contained hits, but no track candidate was found even with a very loose χ^2 criterion, the procedure was retried omitting one plane at a time in hopes of finding an acceptable candidate.

In the horizontal coordinates the bending of the tracks in the magnetic field resulted in one less constraint in the track fitting. Thus, added precautions were necessary to avoid constructing tracks from uncorrelated hits. Candidate tracks were required to point back to the LH_2 target and to bend towards the magnet center line. Candidates with hits in only three MWPC planes were considered only if the fourth plane was empty. All candidate tracks that passed these requirements were accepted. If there were more than 16 combinations on either side, the event was rejected. This cut discarded 4% of the events. A crude momentum was calculated using the bend angle and a constant integral for the magnetic field.

The next step was to pair each candidate in the vertical projection, in turn, with each candidate in the horizontal projection on a given side. This pairing defined candidate particle trajectories that were parametrized by their x and y coordinates and their three-momentum components at the first MWPC plane. If there were more than eight such candidates on a side, the event was rejected. Another 2% of the candidates failed this cut.

The best-fit trajectory was found for each candidate by an iterative procedure. A stepping routine and an approximate map of all magnetic-field components were used to generate a trajectory from the starting parameters. The actual chamber coordinates were compared to the calculated trajectory and a χ^2 was calculated using chamber resolutions determined from the Monte Carlo (Sec. IV). A χ^2-minimization routine was used to find values for the parameters that described the best-fit trajectory. The trajectories on each side with the smallest χ^2 were retained. The parameters of these trajectories were then recalculated using the stepping routine and a detailed magnetic-field map. A track was accepted at this stage if the χ^2 per degree of freedom (DF) was less than 50. The measured chamber efficiencies for accepted tracks were typically 95%.

If acceptable tracks were found on both sides, the trajectories were extrapolated upstream to find their intersection point in the x-z plane. Because the tracks could have only small components of y momentum, this was effectively the point of closest approach (d_A).

The track-finding algorithms were checked both by quantitative tests and qualitatively by comparing the computer results for pattern recognition with those of physicists. Possible track-finding errors could be caused by an extra hit near the real track since the first-pass analysis used a constant-field-integral approximation. By examining events with more than one possible track, it was found that the same trajectory had the best χ^2 using either the approximate magnetic field or the more detailed magnetic-field map.

Events in which extra hits were near a track and the real hit was missing were vulnerable to track-finding er-

rors. The ability of the programs to reject these events and to choose correctly between two hits in a plane that were close together was demonstrated by examining a sample of events with good tracks and no extra or missing hits. The χ^2 per DF rises quite rapidly if any hit was moved from its measured position. This is true even if a hit in another chamber in that coordinate is dropped from the fit. Typical values are a rise in χ^2 per DF of 2 for a 2-mm shift.

To check that eliminating events too complicated to be reconstructed did not bias the data set, we compared events having less than five hits in all planes to those having up to eight hits in at least one plane. No difference in the final distributions were noted for these more complicated events. Using this same comparison to place a limit on the possible excess of complicated events with large χ^2, we conclude that less than 0.2% of the events contain a spurious track. We concluded that the reconstruction programs were close to 100% efficient and this is confirmed by the overall efficiency of the experiment (see Sec. V C).

IV. MONTE CARLO SIMULATION

Even if the data analysis succeeded in selecting a pure sample of e^+e^- pairs, for most events it was impossible to determine whether they resulted from some π^0 decay mode (and from which specific mode) or from another process. Thus, a Monte Carlo simulation of the experiment was required to permit a separation of the modes on a statistical basis. It is essential that this simulation adequately reproduce the dynamics and kinematics of each process as well as the geometry of the experiment. In the list below, the particle(s) that were followed through the apparatus are underlined:

$$\underline{\pi^-}p \rightarrow \underline{\pi^-}p \quad (1)$$

$$\rightarrow \pi^-\underline{p} \quad (2)$$

$$\rightarrow \underline{\pi^0}n,\ \underline{\pi^0} \rightarrow \underline{e}^+\underline{e}^- \quad (3)$$

$$\rightarrow \gamma\underline{e}^+\underline{e}^- \quad (4)$$

$$\rightarrow \underline{e}^+e^-\underline{\gamma} \searrow e^+\underline{e}^- \quad (5)$$

$$\rightarrow \gamma \searrow \underline{e}^+e^- \qquad \gamma \searrow e^+\underline{e}^- \quad (6)$$

$$\rightarrow \underline{e}^+e^-e^+\underline{e}^- \quad (7)$$

$$\rightarrow n\underline{e}^+\underline{e}^- . \quad (8)$$

Modes (1) and (2) were included since the data sample contained some elastically scattered π's and p's that served as a check on the absolute-momentum scale. The π and p were processed separately since the kinematics of elastic scattering allowed only one particle from a single event to traverse the apparatus. Modes (3) through (7) simulated all known processes that contributed significantly to the spectrum of e^+e^- pairs from π^0 decays in the data.

All modes began with a π^- beam with momentum, spatial, and angular distributions corresponding to the measured distributions of the beam. The momentum and direction of the π^0 were selected according to a fit to measured charge-exchange cross sections.[22] The interaction point along the length of the hydrogen target was chosen randomly, taking into account the attenuation of the incident beam.

The angular distribution of the $\pi^0 \rightarrow e^+e^-$ decay [mode (3)] was isotropic in the π^0 center of mass, but was restricted to angles that had a chance of matching the acceptance of the apparatus. Each lepton was propagated through the apparatus. Whenever a particle encountered material, the effects of ionization loss, multiple scattering, and bremsstrahlung were included.[23] The magnetic field used for the simulation was that obtained from a detailed three-dimensional map of the spectrometer magnet. If a particle failed to hit the fiducial region of a chamber or suffered a hard bremsstrahlung, etc., the program recorded the reason for failure and began with a new π^-.

The remaining decay modes [modes (4) through (7)] were processed identically to mode (3) once two leptons were generated. Mode (4) is normal Dalitz decay with the region $0.7 < X \leq 1.0$ being considered, where $X = M/m_{\pi^0}$ is the electron-positron effective mass in units of m_{π^0}. The distributions of X and energy partition were taken from detailed quantum electrodynamic calculations including radiative corrections.[24,25] For mode (5), Dalitz decay with $X < 0.3$ was relevant. In this case, one lepton came from internal conversion and the other from the real photon. Both pair production and Compton scattering were included. Mode (6) considered the dominant π^0 decay mode into two photons and mode (7) took into account double Dalitz decay. The contributions from all of these decay modes were similar since the probability of external photon conversion was about the same as internal conversion. Only energetic leptons from Dalitz decay, from very asymmetric pair production, or from Compton scattering could trigger the apparatus.

One other process was considered, $\pi^-p \rightarrow ne^+e^-$, called inverse electroproduction. The dynamics were described by a code based on a theoretical treatment of electroproduction and related processes.[26] The code calculated cross sections as a function of the total energy in the πp center of mass, the mass squared of the e^+e^- system, a parameter that determined the energy sharing between the e^+ and e^-, the angle of the e^+e^- system in the π^-p center of mass, and the angle between the leptonic and hadronic planes. Our simulation sampled the full parameter space and chose candidate events based on tables of the cross sections.

For each Monte Carlo–generated event, the intersections of the particle trajectories with the locations of the chamber planes were recorded. The Monte Carlo events were processed by the same reconstruction routines that were used for the data events. To simulate the data properly, it was necessary to include the effects of chamber resolution and chamber inefficiencies. Hits were randomly omitted in accordance with the measured chamber inefficiencies. Correlations between missing hits were present in the data, but were not important and were ignored. The chamber resolutions were found by displacing Monte Carlo–generated hits with a Gaussian resolution function and comparing the resulting distributions for χ^2 of the fit and deviations of the hits from the fit trajectory with those from the data. It was found that $\sigma = 0.8$ mm gave a good representation for the front chambers.

In the rear chambers, it was necessary to make allowance for additional effects such as multiple hits in a single delay line or poor timing due to low pulse heights. Other processes that are not included explicitly in the

Monte Carlo program but are simulated adequately by a degraded rare-chamber resolution for some events include Bhabha scattering, Möller scattering, nuclear scattering, and uncorrelated extra tracks traversing the rear MWPC's. If such an extra track passes through the region spanned by the same delay line as the desired track, only one hit would be recorded, but the position of this hit could be anywhere between the real positions of the two tracks. It was found that $\sigma=1.1$ mm for the delay-line planes was appropriate for most of the data and that $\sigma=9.1$ mm for 12% of the hits accounted for effects that degraded the resolution. The resulting rms resolutions as determined from the Monte Carlo were $\Delta p/p=1.8\%$ and $\Delta\cos\theta_{+-}/\cos\theta_{+-}=1.4\%$.

V. FINAL ANALYSIS AND RESULTS

A. Comparison of data and Monte Carlo simulation

The determination of the branching ratio for $\pi^0\to e^+e^-$ depends upon a detailed comparison of the distributions of the square of the e^+e^- effective mass (M^2) for the data and for the Monte Carlo simulation. As was described above, great care was taken to ensure that the Monte Carlo accurately simulated the experiment. In the discussion below, various distributions are compared both to demonstrate the quality of the simulation which is essential to the credibility of our result and to delineate cuts which have been applied to both samples.

The χ^2 distributions for the data and the Monte Carlo are shown in Fig. 4. The agreement for small values of χ^2 ($\chi^2/\mathrm{DF}<4$) tests the correctness of the simulation of the chamber resolutions, the multiple scattering and energy loss suffered by particles traversing material, and the magnetic-field map used in the reconstruction. The width of the χ^2 distribution depends on the weights used for the hits in the fitting program. These weights corresponded to the chamber resolution only while the χ^2 values include the effects of momentum losses and multiple scattering. Both the data and Monte Carlo distributions are ~ 1.4 times the theoretical width due to these effects. Figure 4 also clearly shows an excess of data events with large χ^2 compared to the theoretical χ^2 distribution. The Monte Carlo adequately reproduces the distribution of events with large values of χ^2 for each DF. This confirms that these are real events with poor resolution rather than random hits formed into tracks since the latter would mostly populate the high-χ^2 portions of the distribution with 1 DF. The relative normalization for 3 DF and 2 DF is fixed, which demonstrates that the Monte Carlo includes chamber inefficiencies correctly. An adjustment of the normalization was required for 1 DF to account for correlated inefficiencies. The cut on χ^2 was chosen to include most data events with reasonable resolution and was made at the same point on the theoretical χ^2 distribution for each DF, i.e., the point that would include 99% of an ideal distribution. There were 16 667 data events surviving this cut defining valid tracks.

The second category of cuts defined a fiducial volume for the apparatus. It included cuts on an acceptable region of each chamber plane. The cuts were made on the position of the trajectory rather than the position of the hits to avoid any problems caused by missing hits. A cut was also made on the intersection of the trajectory and the

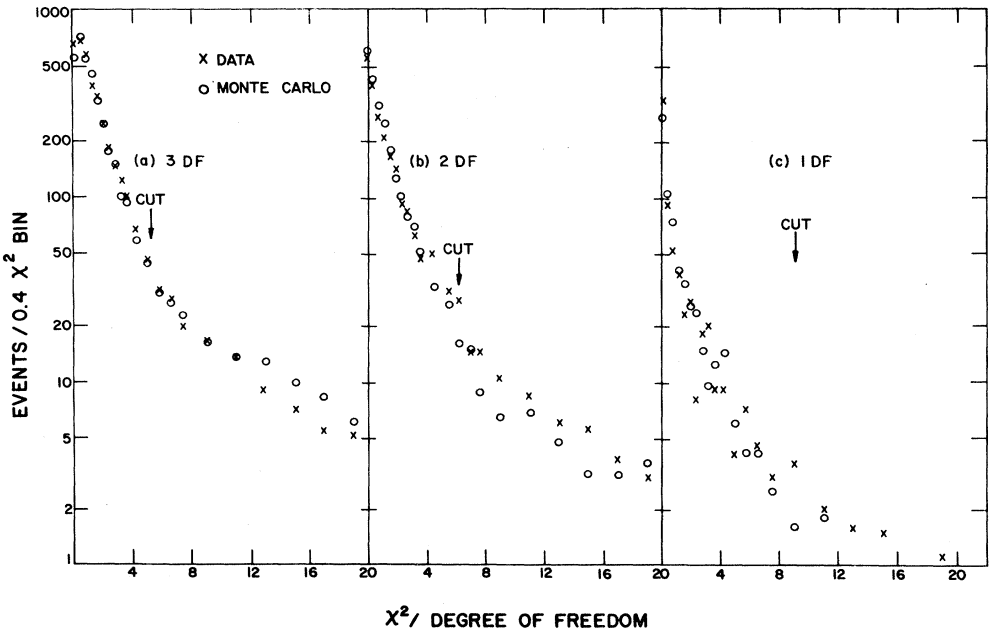

FIG. 4. Distribution of χ^2 values for track fits with 1, 2, and 3 degrees of freedom. The circles are from the Monte Carlo simulation.

Cherenkov-counter mirror. By comparing x and y distributions for data and Monte Carlo at this z location, it was found that the Cherenkov counter efficiency was lower near the beam line. A fraction of Monte Carlo—generated events in this region were deleted to compensate for this effect. At this point the number of data events that survived was 7037.

The cuts to eliminate accidental coincidences were applied to the interaction point (required to be within the target volume), to the sum of the lepton energies (required to be less than 340 MeV), to the agreement between the trajectory and the counters that fired, and to the distance of closest approach d_A. Figure 5 shows the distribution of d_A for the data. The Monte Carlo distribution is shown in Fig. 6. To compare the data and Monte Carlo distributions, it is necessary to know the d_A distribution for uncorrelated tracks. This was obtained from a special analysis run using e^+ tracks and e^- from different events and is shown in Fig. 6. The relative normalization of the distribution for accidentals and for Monte Carlo events was chosen for a best fit to the data distribution. The combined spectrum is shown in Fig. 5. Since d_A depends strongly on the assumed chamber resolution and multiple scattering, the agreement between these two distributions is another confirmation of the accuracy of the Monte Carlo simulation. The location of the cut on d_A is shown in Fig. 5. After these cuts 3886 events remained.

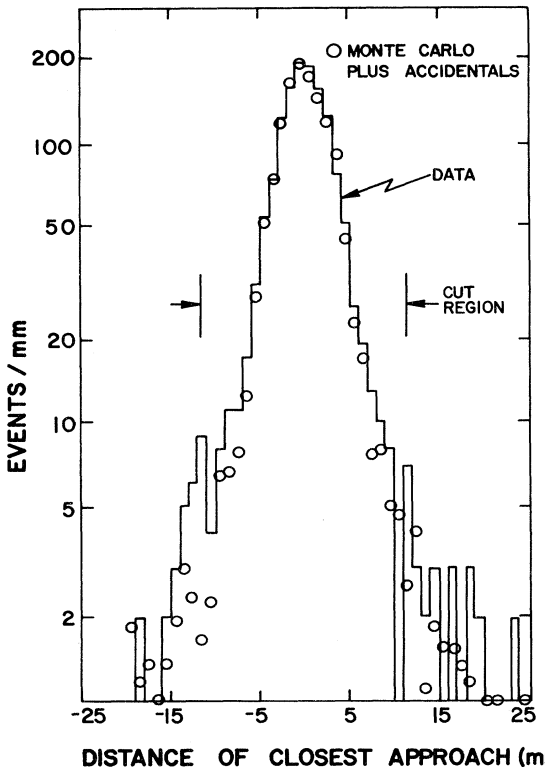

FIG. 5. Distribution of distance of closest approach, d_A, for tracks from events that passed other cuts required of good events. The circles show the distribution for the sum of the Monte Carlo and accidentals from Fig. 6.

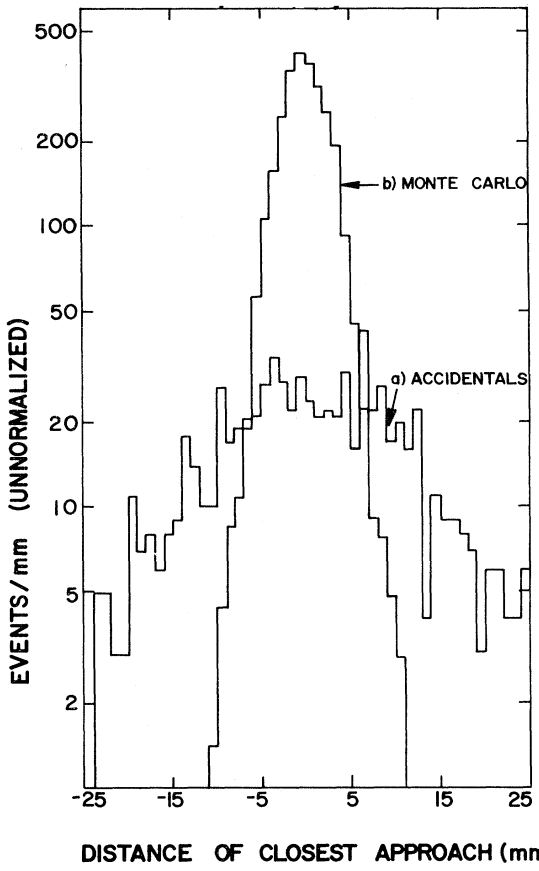

FIG. 6. Distributions of distance of closest approach d_A for (a) accidentals and (b) Monte Carlo simulation.

A final cut was applied that eliminated events with low effective mass that could not contribute to the signal. This cut required the sum of the energies of the e^+ and e^- to be greater than 290 MeV and was satisfied by 1330 events.

In addition to the comparisons listed above there are other checks that were made. Data were taken with the LH_2 target empty for about 10% of the running time. None of the candidate events from the target empty sample survived all of the cuts. Also the data taken with both polarities of the magnet were compared and no differences were found.

It is important to know that the two particles in each event are an electron and a positron. While protons could easily be identified in the raw sample of tracks from their large pulse heights in the scintillation counters, essentially none survived to the final data set. Similarly, a clear peak due to pions was present in the momentum distribution before cuts, but none is seen in the final distribution. Further, the pulse-height distribution from the Cherenkov-counter photomultiplier tubes confirms that the events which survive are electrons as shown in Fig. 7.

Two checks of the absolute momentum scale are shown

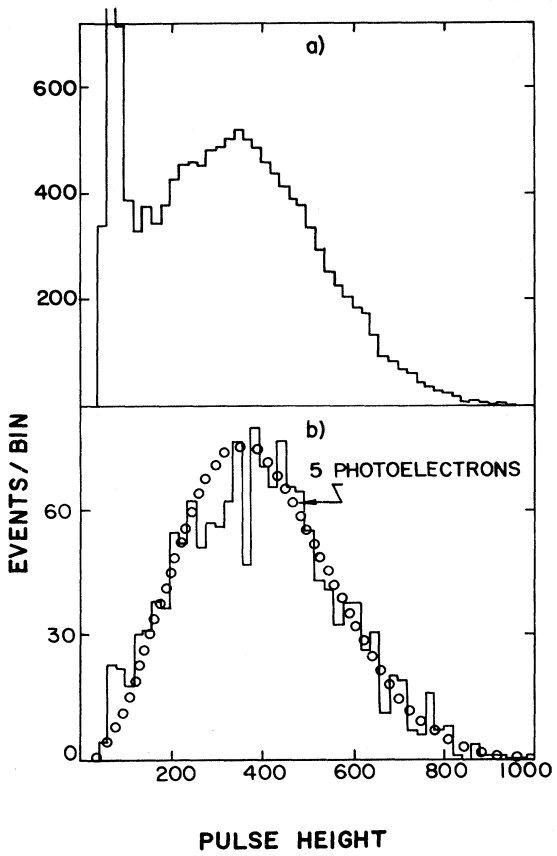

FIG. 7. Pulse-height distribution from one Cherenkov-counter photomultiplier tube. (a) Raw data. The peak at small pulse height corresponding to one photoelectron is due to pions and protons in the data. (b) Accepted events. The circles indicate the shape of the distribution expected from a Poisson distribution with $N=5$ photoelectrons.

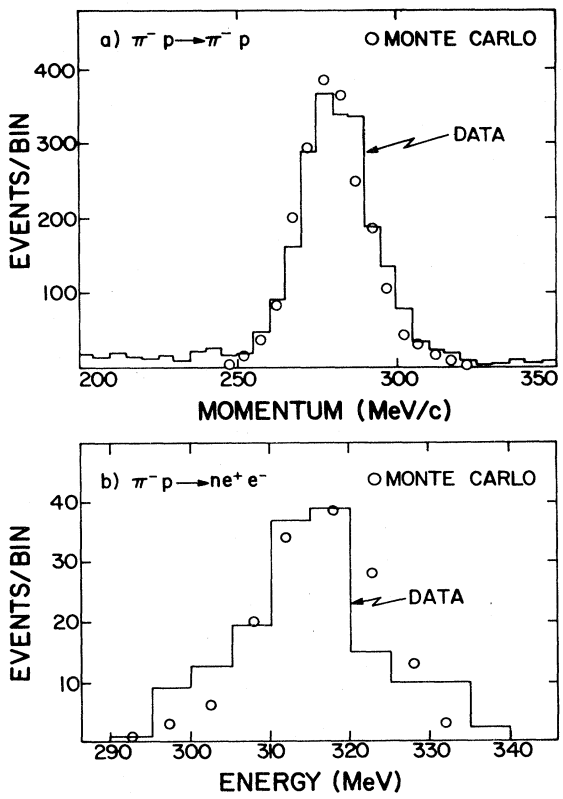

FIG. 8. Comparison of Monte Carlo and data distributions for (a) pion momentum for elastically scattered pions, and (b) total energy of the leptons for $\pi^- p \to nee$ events with $M^2 \geq 19\,000$ $(\mathrm{MeV}/c^2)^2$. The centroids of the peaks agree to better than 1% in both cases.

in Fig. 8. The momentum distribution of pions from elastic $\pi^- p$ scattering from the data and from the Monte Carlo are displayed in Fig. 8(a). The sum of lepton energies for $\pi^- p \to nee$ events with invariant mass above m_{π^0} $[M^2 \geq 19\,000$ $(\mathrm{MeV}/c^2)^2]$ is shown in Fig. 8(b). The close agreement between the data and Monte Carlo distributions in both cases confirms the absolute momentum scale, both of the spectrometer and of the incident beam, and checks the assumed chamber resolutions.

B. Fitting the e^+e^- effective-mass distribution

A histogram showing M^2 for all of the data subjected to the cuts described above is shown in Fig. 9. A large $\pi^0 \to e^+e^-$ signal would have resulted in a bump centered at $M^2 \simeq 17\,700$ $(\mathrm{MeV}/c^2)^2$ with a FWHM of $\simeq 1500$ $(\mathrm{MeV}/c^2)^2$. The bump would be at a value of M^2 smaller than $m_{\pi^0}{}^2$ due to the energy losses suffered by the electrons and positrons in the target and the spectrometer. Even without a visible bump a substantial contribution from $\pi^0 \to e^+e^-$ is possible.

The shape of the M^2 distribution for the signal and each

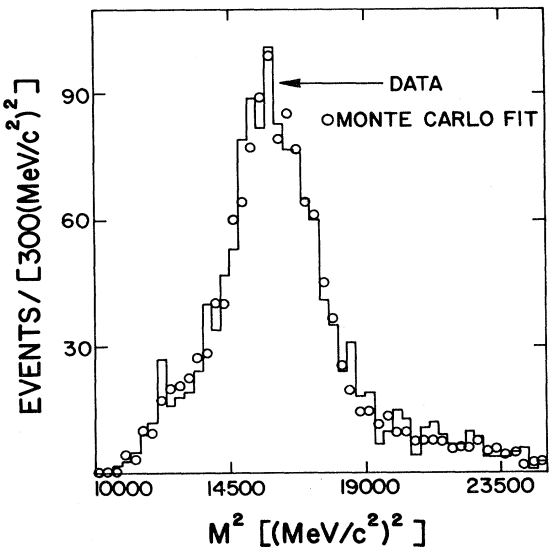

FIG. 9. Distribution of the square of the effective mass for accepted e^+e^- pairs. $(m_{\pi^0})^2$ appears at 17 700 $(\mathrm{MeV}/c^2)^2$ due to energy losses by particles traversing the target and the spectrometer. The sum of the components from Fig. 11 is shown as the circles.

background process is given by the Monte Carlo simulation shown in Figs. 10 and 11. The distributions for the dominant π^0 decay modes are shown in Fig. 10. The two modes that involve conversion of a real photon contribute more events at high M^2 than the modes resulting from internal conversion due to the high probability of maximum energy transfer to the electron in Compton scattering. The tail of these distributions extends above $m_{\pi^0}{}^2$ due to the resolution of the experiment. The distributions are truncated at lower M^2 by the cut that eliminated events with significant missing energy. The relative normalizations of these modes are fixed by the known π^0 branching ratios and the known probability for photon conversion via pair production and Compton scattering in the available material. Figure 11(a) shows the mass spectrum for $\pi^0 \to e^+e^-$; the shape of this distribution gives the M^2 resolution of the experiment. The Monte Carlo–generated M^2 distribution for $\pi^- p \to n e^+ e^-$ is shown in Fig. 11(c). Since the input spectrum varies slowly with mass, this distribution illustrates the M^2 acceptance of the apparatus.

The total number of accidental e^+e^- coincidence events in the data sample was obtained by using the d_A distribution of uncorrelated tracks in Fig. 6. The result was that $(5\pm1)\%$ of the data sample within the d_A cut was due to accidental coincidences. The M^2 distribution for these accidental coincidence events was taken to be that of events with $1.0 < |d_A| < 3.0$ cm. This distribution is shown in Fig. 11(b). The contribution from accidental coincidences was then subtracted from the data.

The relative strengths of the normal π^0 decay modes,

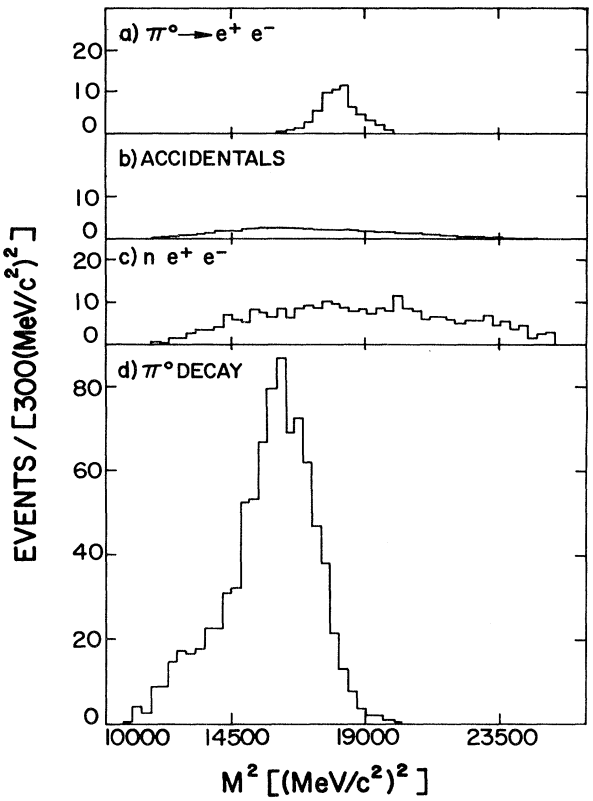

FIG. 11. Normalized contributions of Monte Carlo–generated modes when fitted to the data distribution. The distribution in (d) is the sum of the four π^0 decay modes in Fig. 10.

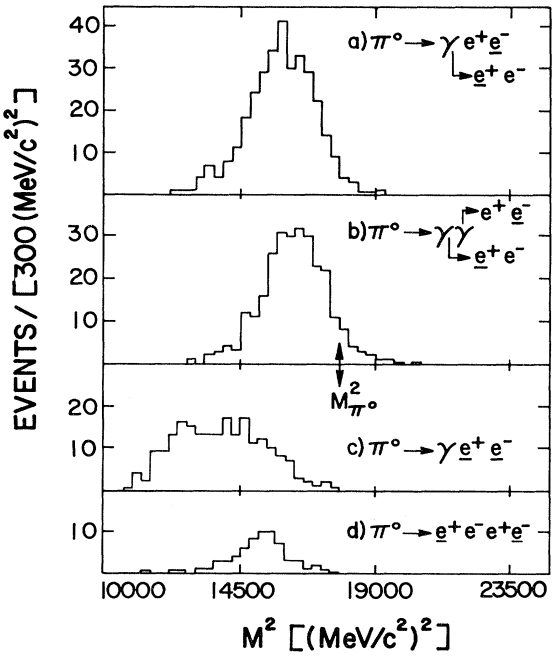

FIG. 10. M^2 distributions of the various decay modes from the Monte Carlo simulation. The relative normalizations are fixed by known π^0 branching ratios and photon conversion probability.

the $\pi^0 \to e^+e^-$ signal, and the $\pi^- p \to n e^+ e^-$ signal were determined by comparing the Monte Carlo–generated M^2 distributions for these processes with that for the data. A fitting program determined those relative strengths that led to a least-squares fit to the M^2 distribution of the data. The best fit is shown in Fig. 9. The normalized contributions from each mode to this fit are shown in Fig. 11. The best fit has 59 ± 21, $\pi^0 \to e^+e^-$ events and a χ^2 of 42 for 47 DF. This shows that the fit represents the data very well. The statistical error in the signal corresponds to the variation required to increase the χ^2 by 1. Fixing the $\pi^0 \to e^+e^-$ signal to either 0 or 120 events increases the χ^2 by 7 with 1 additional DF. Although the best fit is significantly better than the fit with no signal, it is impossible to exclude a null result from our data. The results presented here are consistent with our previously published result.[27] The only difference is a change in the chamber resolutions in the Monte Carlo simulation that reproduces the data events with large χ^2 for the track fits.

We have studied the stability of the $\pi^0 \to e^+e^-$ signal with respect to possible uncertainties in the relative mass scales of the data and Monte Carlo simulation. The mass scale of the Monte Carlo spectra is known with negligible uncertainty. The mass scale for the data depends on an absolute knowledge of the momentum and opening-angle scales which come from a detailed map of the magnetic

field and the measured locations of the chamber planes. To study the effect of uncertainty in absolute chamber positions, several displacements of chamber positions were tried. For example, moving the last chamber away from the beam line by 1.5 mm and adjusting the other chambers to maintain fits to the straight-line data, the momentum increases by 0.3% and the change in $(1-\cos\theta_{+-})$ is -0.2%. This corresponds to a shift in M^2 scale of 20 $(\mathrm{MeV}/c^2)^2$.

By trying several sets of possible absolute and relative chamber locations and including the uncertainty in our knowledge of the absolute magnetic field ($<0.1\%$), we estimate an upper limit on the difference between the M^2 scales for data and Monte Carlo of 40 $(\mathrm{MeV}/c^2)^2$. This could result in a change in the signal of $<\pm 15\%$.

The absolute momentum scale was confirmed at the 1% level in two ways. The first was from our knowledge of the beam momentum and the reconstructed momenta of elastically scattered pions. The second was from the sum of lepton energies for those $\pi^- p \to nee$ events with an invariant mass above the pion mass. The accuracy of these comparisons is limited by the uncertainty in the absolute incident-beam momentum and thus is inferior to our knowledge of the absolute momentum scale discussed above.

Other changes in the $\pi^0 \to e^+e^-$ signal can result from cuts or normalization factors. There is no significant difference in the M^2 distributions for events with large χ^2 and those with small χ^2. Removing the cut on the sum of the two lepton energies raises the deduced $\pi^0 \to e^+e^-$ signal by 10%. The conversion probability, averaged over photon energy and material traversed, was $(1.96\pm0.05)\times10^{-3}$; the error is dominated by the uncertainty in the amount and composition of the material traversed. This leads to a 2% systematic uncertainty in the $\pi^0 \to e^+e^-$ signal. The fit assumed a neutral-pion electromagnetic-form-factor slope[28] $a=0.11\pm0.03$ for the Dalitz decay mode. The experimental error in the form-factor slope results in a 3% uncertainty in the $\pi^0 \to e^+e^-$ signal. Finally, the uncertainty in the number of accidental coincidences in the data sample implies a 1% uncertainty in the $\pi^0 \to e^+e^-$ signal.

In summary, we see statistically significant evidence for the decay $\pi^0 \to e^+e^-$ which is insensitive to large changes in the event selection criteria and to assumptions concerning the background processes and strengths. Visual evidence for the presence of a $\pi^0 \to e^+e^-$ signal in the data is shown in Fig. 12. The region $16\,300 \le M^2 < 19\,300$ $(\mathrm{MeV}/c^2)^2$ was excluded and the backgrounds were fit to the remaining M^2 bins of the data. The background distribution was subtracted from the data for all bins and the difference is plotted in Fig. 12. There is a significant excess of data events with mass values near $m_{\pi^0}{}^2$ after the fitting procedure minimized the difference outside the excluded region. The normalized $\pi^0 \to e^+e^-$ signal is superimposed on this spectrum.

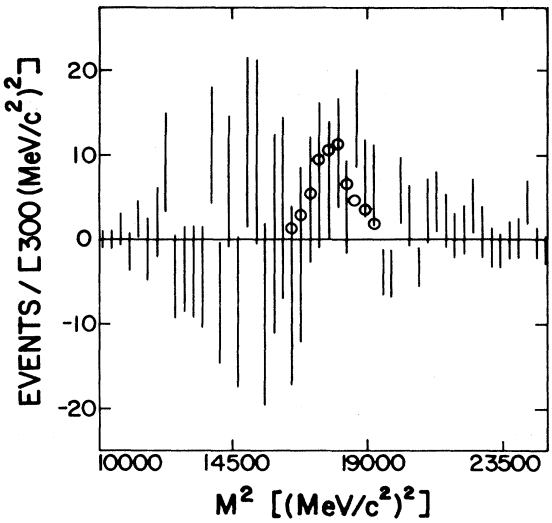

FIG. 12. Data minus Monte Carlo simulation with the $\pi^0 \to e^+e^-$ signal region excluded from the fit (see text). The open circles represent the signal of 59 $\pi^0 \to e^+e^-$ events.

C. Normalization

There are several ways to convert the observed number of $\pi^0 \to e^+e^-$ events into a branching ratio. One could normalize to the dominant π^0 decay modes [modes (4) through (7)] or to the $\pi^- p \to ne^+e^-$ mode. Alternatively, one could combine the number of incident negative pions, the known charge-exchange cross section, and the acceptance of the apparatus as calculated from the Monte Carlo code to determine the normalization. Of these, a normalization to the dominant π^0 decays is the most straightforward since the incident-beam intensity, target length and density, charge-exchange cross section, and overall apparatus and reconstruction efficiencies cancel by forming the ratio. We did not use the $\pi^- p \to ne^+e^-$ yield for normalization since the production cross section is not well known.[29]

To normalize to the dominant π^0 decay modes, we first calculate the number of π^0's produced in the target divided by the overall efficiency of the apparatus and analysis. Since π^0's produced at angles greater than 30° in the $\pi^- p$ center of mass cannot trigger the apparatus, the production is calculated for 0° to 30°. From the fit, there were 888 ± 42 events from dominant π^0 decays in the data. Dividing this number by the sum of the Monte Carlo acceptances for these modes yields $(1.83\pm0.10)\times10^{11}$ π^0's. Using this number of π^0's and the Monte Carlo acceptance for $\pi^0 \to e^+e^-$ $[(1.93\pm0.03)\times10^{-3}]$ for π^0's produced from 0° to 30° in the center of mass, the 59 ± 21 events imply

$$B_{\pi^0}=\frac{\Gamma(\pi^0 \to e^+e^-)}{\Gamma(\pi^0 \to \gamma\gamma)}=(17\pm6\pm3)\times10^{-8}\,,$$

where the first error is due to the statistical uncertainties in both the data and the Monte Carlo. The second error reflects our estimate of an overall systematic uncertainty of 18%.

As a check of the normalization, we can calculate the number of π^0's incident on the apparatus from the number of incident π^- (Sec. II B 3), the target length (Sec. II B 1), and the charge-exchange cross section (Ref. 22). This calculation yields $(2.16\pm0.22)\times10^{11}$ π^0's incident on the ap-

paratus from 0° to 30° in the center of mass. The product of this number and the overall apparatus and reconstruction efficiency should equal the number of π^0's deduced above from the observed number of π^0 decay events. This is true if the overall apparatus and reconstruction efficiency equals (0.85 ± 0.10) which agrees with our best estimate. This number reflects the effects of the Cherenkov-counter efficiency, the electronics dead time, and the reconstruction algorithm. The effect of the χ^2 cut on tracks, and the chamber efficiencies were included explicitly in the Monte Carlo.

VI. DISCUSSION

Our result is almost four times the unitarity limit while existing calculations generally predict B_{π^0} is less than twice the unitarity value. The two recent quark-model calculations use different treatments of the $q\bar{q}$ binding and predict $B_{\pi^0}=6.2\times10^{-8}$ in one case[6] and 6.3×10^{-8} in the other.[7] Both calculations indicate that the contribution from the real part of the amplitude is small. Nevertheless, it is possible that "exotic" contributions may be significant in $\pi^0\to e^+e^-$ and not for the other pseudoscalar-meson decays.[6] An important question is then whether B_{π^0} is really much larger than the unitarity lower limit. To show this with greater certainty, one would need an experiment with significantly smaller errors.

As was mentioned in Sec. IV, radiative corrections for Dalitz decay [mode (4)] were explicitly included in the Monte Carlo simulation. This was important because the radiative corrections decrease the number of events with large X, which are just those that contribute to the data sample. Other radiative corrections are small. The major effect of these corrections to pair production[30] is to increase the total cross section by 0.9%. The radiative corrections to Dalitz decay with small X [mode (5)] and double Dalitz decay [mode (7)] have a negligible impact on our result.

The radiative corrections to $\pi^0\to e^+e^-$ itself have been calculated by Bergström.[31] The experimental result presented above excludes events with hard photons from internal bremsstrahlung. In our Monte Carlo code for $\pi^0\to e^+e^-$, all events start with $M=m_{\pi^0}$. If we generate events with $0.9m_{\pi^0}{}^2\le M^2\le m_{\pi^0}{}^2$ according to the distribution of Ref. 31, the M^2 spectrum for $\pi^0\to e^+e^-$ changes slightly, but we find a negligible change in both the number of $\pi^0\to e^+e^-$ events and the quality of the least-squares fit to the M^2 distribution of the data. Events with more energetic photons would not contribute to the $\pi^0\to e^+e^-$ signal. The measured branching ratio for $\pi^0\to e^+e^-$ would have to be increased by 7.4% to include these events. We conclude that the effects of radiative corrections are small compared to the statistical uncertainty of our result.

In this experiment the uncertainty in the branching ratio for $\pi^0\to e^+e^-$ is dominated by the statistical error in the estimate of the number of background events in the vicinity of the signal. As can be seen from Fig. 11, the major contribution comes from the other π^0 decay modes. For the region $16\,600\le M^2\le 19\,000$ $(\mathrm{MeV}/c^2)^2$, the best fit indicates that of the 340 observed events, 195 arise from other π^0 decay modes and only 67 from $\pi^-p\to ne^+e^-$. Almost all of the events from the other π^0 decay modes are the result of a photon conversion [modes (5) and (6) in Sec. IV]. In particular, the contribution from large-X Dalitz decay [mode (4)], which has been discussed as an important background,[20] is small in comparison. Only five events come from Dalitz decay [mode (4)] and three events come from double Dalitz decay [mode (7)]. Thus, to substantially reduce the backgrounds, one would have to reduce the amount of material available for photon conversion. The vast majority of the photon conversions take place in the liquid hydrogen (71%) and the target flask and vacuum window (25%). The remaining conversions occur in the air between the target and the first MWPC, and the material of the first MWPC. It is difficult to imagine how the amount of material in the target could be substantially reduced. A shorter target would improve the signal-to-noise ratio somewhat but at the expense of the number of $\pi^0\to e^+e^-$ events per incident pion.

The statistical precision of the experiment would be improved if the M^2 resolution were better. Unfortunately, the contributions to the resolution from multiple scattering in the hydrogen target, the target flask and vacuum window, the MWPC's, and from the MWPC resolutions are all similar. A large reduction in one of these contributions would not markedly improve the overall M^2 resolution. Another experiment,[32] in progress, also used $\pi^-p\to\pi^0n$ at 300 MeV/c and should obtain a measurement of B_{π^0} with precision similar to ours.

Using the reaction $K^+\to\pi^+\pi^0$ to provide a tagged source of π^0's in vacuum[16] appears to be the cleanest way to measure the $\pi^0\to e^+e^-$ branching ratio. In Ref. 16, about six $\pi^0\to e^+e^-$ events were observed with a background of only one event in a beam of 7×10^4 K^+/sec at 2.8 GeV/c. An experiment[33] in a higher-flux K^+ beam should be able to significantly improve the accuracy of the measurement of B_{π^0} and determine whether it remains in disagreement with conventional calculations.

ACKNOWLEDGMENTS

We wish to thank the LAMPF staff and our many colleagues who assisted in the execution of this experiment. Charlie Dalton, Ron Harrison, George Krausse, and Dick Werbeck helped in constructing and installing the apparatus. Jan Novak designed the liquid-hydrogen target; Grace Perez assisted in running the experiment. Steve Dam, John Faucett, Peter Gram, Brian Henderson, Sue Willis, John Wood, and especially Sue Johnson, made valuable contributions to the data analysis. Peter Herczeg, Darragh Nagle, Lars Bergström, and Terry Goldman provided valuable comments on the manuscript. This work was supported by the U. S. Department of Energy and Associated Western Universities, Inc.

*Present address: Brookhaven National Laboratory, Upton, New York 11973.

†Present address: Diasonics, Inc., 1545 Barber Lane, Milpitas, California 95035.

[1]S. M. Berman and D. A. Geffen, Nuovo Cimento 18, 1192 (1960).

[2]S. D. Drell, Nuovo Cimento 11, 693 (1959).

[3]C. Quigg and J. D. Jackson, Lawrence Radiation Laboratory Report No. UCRL-18487, 1968 (unpublished).

[4]I. K. Litskevich and V. A. Franke, Yad. Fiz. 10, 815 (1969) [Sov. J. Nuc. Phys. 10, 471 (1970)].

[5]M. Pratap and J. Smith, Phys. Rev. D 5, 2020 (1972).

[6]L. Bergström, Z. Phys. C 14, 129 (1982).

[7]K. S. Babu and E. Ma, University of Hawaii Report No. UH-511-478-82, 1982 (unpublished).

[8]J. C. Pati and A. Salam, Phys. Rev. D 11, 1137 (1975).

[9]J. D. Davies, J. G. Guy, and R. K. P. Zia, Nuovo Cimento 24A, 324 (1974).

[10]A. Soni, Phys. Lett. 52B, 332 (1974); 53B, 280 (1974).

[11]P. Herczeg, Phys. Rev. D 16, 712 (1977).

[12]H. E. Haber, G. L. Kane, and T. Sterling, Nucl. Phys. B161, 493 (1979).

[13]P. Herczeg (private communication); in Proceedings of the Workshop on Program Options in Intermediate-Energy Physics, Los Alamos National Laboratory Report No. LA-8335-C, 1980 (unpublished).

[14]F. C. Michel, Phys. Rev. 138, B408 (1965).

[15]J. Schacher, G. Czapek, B. Hahn, and T. Marti, Lett. Nuovo Cimento 20, 177 (1977).

[16]J. Fischer, P. Extermann, O. Guisan, R. Mermod, B. Morel, L. Rosselet, R. Sachot, P. Bloch, G. Bunce, B. Devaux, A. M. Diamant-Berger, N. Do-Duc, G. Marel, and R. Turlay, Phys. Lett. 73B, 364 (1978).

[17]B. D. Hyams, W. Koch, D. C. Potter, L. von Lindern, E. Lorenz, G. Lütjens, U. Stierlin, P. Weilhammer, Phys. Lett. 29B, 128 (1969).

[18]V. A. Viktorov, S. V. Golovkin, R. I. Dzhelyadin, A. M. Zaitsev, V. A. Kachanov, A. S. Konstantinov, V. F. Konstantinov, V. P. Kubarovsky, A. V. Kulik, L. G. Landsberg, V. M. Leontiev, V. A. Mukhin, V. F. Obraztsov, and Yu. D. Prokoshkin, Yad. Fiz. 32, 1002 (1980) [Sov. J. Nucl. Phys. 32, 518 (1980)]; also, R. I. Dzhelyadin *et al.*, Phys. Lett. 97B, 471 (1980).

[19]Particle Data Group, Rev. Mod. Phys. 52, S88 (1980).

[20]H. Burkhardt, R. Zia, and J. Davies, J. Phys. A 7, 40 (1974).

[21]M. A. Schardt, J. S. Frank, C. M. Hoffman, R. E. Mischke, D. C. Moir and P. A. Thompson, Phys. Rev. D 23, 639 (1981).

[22]G. Källen, *Elementary Particle Physics* (Addison-Wesley, Reading, Mass., 1964), p. 87.

[23]R. E. Mischke and R. A. Williams, Los Alamos National Laboratory Report No. LA-UR-82-1952, 1982 (unpublished).

[24]D. W. Joseph, Nuovo Cimento 16, 997 (1960).

[25]B. E. Lautrap and J. Smith, Phys. Rev. D 3, 1122 (1971); K. O. Mikaelian and J. Smith, *ibid.* 5, 1763 (1972).

[26]N. Dombey and B. J. Read, J. Phys. G 3, 1659 (1977).

[27]R. E. Mischke, J. S. Frank, C. M. Hoffman, D. C. Moir, J. S. Sarracino, P. A. Thompson, and M. A. Schardt, Phys. Rev. Lett. 48, 1153 (1982).

[28]J. Fischer, P. Extermann, O. Guisan, R. Mermod, L. Rosselet, R. Sachot, P. Bloch, G. Bunce, B. Devaux, A. M. Diamant-Berger, N. Do-Duc, G. Marel and R. Turlay, Phys. Lett. 73B, 359 (1978).

[29]C. M. Hoffman, J. S. Frank, R. E. Mischke, D. C. Moir, J. S. Sarracino, P. A. Thompson, and M. A. Schardt, Phys. Rev. D 28, 660 (1983).

[30]Y-S. Tsai, Rev. Mod. Phys. 46, 815 (1974); K. J. Mork and H. Olsen, Phys. Rev. 140, B1661 (1965).

[31]L. Bergström, CERN Report No. TH.3439-CERN, 1982 (unpublished).

[32]W. van Doesburg, H. Verheul, A. G. Zephat, J. D. Davies, J. Lowe, S. M. Playfer, T. Bressani, M. Caria, E. G. Michaelis, C. W. E. van Eijk, J. Lourens, D. Frame, G. Kernel, F. Sever, A. Stanovnik, J. V. Jovanovich, F. Siohan, N. W. Tanner, J. Harvey, E. Chiavassa, S. Costa, G. Dellacasa, M. Gallio, and A. Musso, paper submitted to the 9th International Conference on High Energy Physics and Nuclear Structure, Versailles, 1981 (unpublished).

[33]M. E. Zeller, D. M. Lazarus, W. E. Cleland, J. A. Thompson, and P. S. Cooper, Brookhaven National Laboratory, AGS Proposal No. 777, 1982 (unpublished).